Inverse RIE Lag during Silicon Etching in SF$_6$ + O$_2$ Plasma

R. KNIZIKEVIČIUS*

Department of Physics, Kaunas University of Technology, 73 K. Donelaičio Str., LT-44249 Kaunas, Lithuania

The reactive ion etching of silicon in SF$_6$ + O$_2$ plasma is considered. The etched trench profiles are calculated as a function of mask dimensions, flux of reactive plasma species, and ion bombardment parameters. It is found that with the increase in O$_2$ content aspect ratio and etching anisotropy initially decrease. 30% O$_2$ in the feed is required to suppress chemical etching of side walls, and to restore the values of aspect ratio and etching anisotropy downgraded by the increased chemical etching. With further increase in O$_2$ content aspect ratio and etching anisotropy increase. Later, the aspect ratio starts to decrease due to the accumulation of SiO$_2$ molecules in the trench bottom and inverse reactive ion etching lag takes place.

1. Introduction

The penetration of fluorine atoms into silicon lattice during the etching process reduces usability of fluorine-based plasmas in the fabrication of integrated circuits. The incorporation of F atoms into the etched structures changes their chemical and electrical properties [1]. The feature size at which fluorine-based plasmas become unusable depends on the intended usage of the etched structures. Nevertheless, the fluorine-based plasmas are very well suited for the formation of larger structures used in nanoelectromechanical systems [2, 3]. The structures etched in SF$_6$ plasma have smooth surfaces and round corners. This prevents void formation during trench refilling and helps to avoid breakdown of the dielectric film covering the trench side walls. Round corners also reduce the build-up of mechanical stress onto a silicon surface [4]. The addition of small amount of O$_2$ gas to SF$_6$ plasma significantly increases silicon etching rate. Chemical reactions responsible for the enhancement of silicon etching rate are well understood [5], and SF$_6$ + O$_2$ plasma is commonly used in through-silicon via applications [6–9]. However, the reduction of silicon etching rate caused by the O$_2$ addition to SF$_6$ plasma is less investigated. A better understanding of etched trench shape dependence on O$_2$ content in the feed will enable more efficient fabrication of nanoelectromechanical systems.

In previous work [10], chemical composition of SF$_6$ + O$_2$ plasma is calculated by extrapolation from the experimental data. The derived concentrations of reactive species are used to investigate one-dimensional chemical etching of silicon in SF$_6$ + O$_2$ plasma. However, two-dimensional reactive ion etching (RIE) of silicon in the plasma was not considered. In this work, the influence of O$_2$ content in the feed on the etched trench profiles

is investigated. It is found that in order to enable anisotropic etching certain O$_2$ content is required to suppress chemical etching of side walls. At high O$_2$ content in the feed, inverse RIE lag takes place due to the accumulation of SiO$_2$ molecules in the trench bottom.

2. Model

During the etching process, competition between F and O atoms for active Si surface sites takes place. The reactions included in the model are the following:

$$\text{Si} + 4\text{F} \rightarrow \text{SiF}_4, \tag{1}$$

$$\text{Si} + 2\text{O} \rightarrow \text{SiO}_2, \tag{2}$$

$$\text{SiO}_2 + 4\text{F} \rightarrow \text{SiF}_4 + \text{O}_2. \tag{3}$$

These processes are characterized by the reaction rate constants k_1, k_2, and k_3, respectively.

The trench bottom is subjected to the ion bombardment, where the activation and physical sputtering of surface particles take place. The activation of Si atoms and SiO$_2$ molecules on the surface are defined by the following reactions: $Si \xrightarrow{\text{ions}} Si^*$ and $SiO_2 \xrightarrow{\text{ions}} SiO_2^*$, which are characterized by the activation frequencies

$$G_i = \frac{g_i I_0}{C}, \tag{4}$$

where g_i is the activation constant of the i-th surface component, I_0 is the ion flux, and C is the concentration of surface atoms ($C = 1.36 \times 10^{19}$ m^{-2}). The activated particles have increased number of dangling bonds. F and O atoms more intensively react with the activated Si atoms and SiO$_2$ molecules, and the following reactions take place:

$$\text{Si}^* + 4\text{F} \rightarrow \text{SiF}_4, \tag{5}$$

$$\text{Si}^* + 2\text{O} \rightarrow \text{SiO}_2, \tag{6}$$

$$\text{SiO}_2^* + 4\text{F} \rightarrow \text{SiF}_4 + \text{O}_2. \tag{7}$$
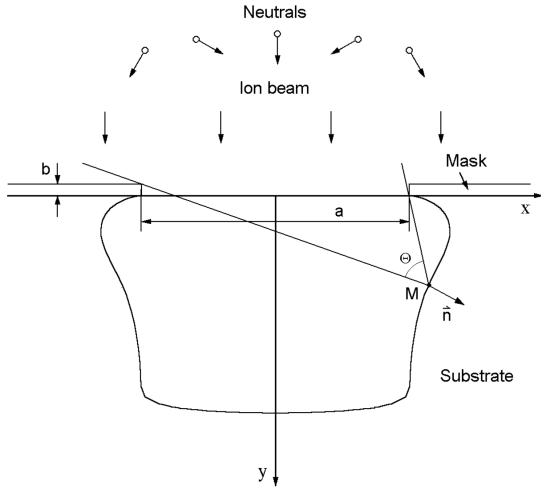
———————

*e-mail: Rimantas.Knizikevicius@ktu.lt

Fig. 1. Schematic presentation of two-dimensional RIE.

These processes are characterized by the reaction rate constants k_4, k_5, and k_6, respectively. SiF_4 molecules are weakly bound to the surface and diffuse in the adsorbed layer until eventually desorb. The desorption frequency is equal to

$$\omega_1 = \nu_0 \exp\left(\frac{-E_d}{kT}\right), \tag{8}$$

where ν_0 is the lattice atom oscillation frequency, E_d is the desorption activation energy, k is the Boltzmann constant, and T is the temperature. Let us assume that formed O_2 molecules instantly desorb.

The activated Si atoms and SiO_2 molecules are sputtered by low energy incident ions. Sputtering of the Si^* atoms and SiO_2^* molecules is characterized by the sputtering frequencies

$$\omega_i = \frac{Y_i I_0 f(\alpha)}{C}, \tag{9}$$

where Y_i is the sputtering yield of i-th component, $f(\alpha) = \cos^{0.5}\alpha$ is the sputtering yield dependence on the incident ion angle α measured from the surface normal. The activated surface particles relax, and the following reactions take place: $Si^* \rightarrow Si$, $SiO_2^* \rightarrow SiO_2$. These processes are characterized by the relaxation frequencies

$$R_{r,i} = \frac{1}{\tau_i}, \tag{10}$$

where τ_i is the mean relaxation time of i-th component. Let us assume that $R_{r,i} = R_r$.

SiF_4 molecules, produced during reactions on the surface, are included in the adsorbed layer of one-monolayer thickness. The relative concentration of SiF_4 molecules is equal to $c_1 = [SiF_4]/C$. Four components exist on the surface: Si, SiO_2, Si^*, and SiO_2^* with relative concentrations $c_2 = [Si]/C$, $c_3 = [SiO_2]/C$, $c_4 = [Si^*]/C$, and $c_5 = [SiO_2^*]/C$. The relative concentrations of surface components must fulfill the condition: $\sum_{i=2}^{5} c_i = 1$. The following system of differential equations describes kinetics of component concentrations in the adsorbed layer and on the surface:

$$\begin{cases} \frac{dc_1}{dt} = R_1\beta c_2 + R_3\beta c_3 + R_4\beta c_4 + R_5\beta c_4 - \omega_1 c_1, \\ \frac{dc_2}{dt} = -G_2 c_2 - R_2\beta c_2 + R_3\beta c_3 + R_4\beta c_4 + R_6\beta c_6 \\ \quad + R_r c_4 + \omega_4 c_4 + \omega_5 c_5, \\ \frac{dc_3}{dt} = -G_3 c_3 + R_2\beta c_2 - R_3\beta c_3 + R_5\beta c_4 + R_r c_5, \\ \frac{dc_4}{dt} = G_2 c_2 - R_4\beta c_4 - R_5\beta c_4 - R_r c_4 - \omega_4 c_4, \\ \frac{dc_5}{dt} = G_3 c_3 - R_6\beta c_6 - R_r c_5 - \omega_5 c_5, \end{cases} \tag{11}$$

where $\beta = 1 - \Theta$ is the fraction of the surface not covered with adsorbate, $\Theta = c_1$ is the surface coverage, $R_1 = k_1 n_F^4$, $R_2 = k_2 n_O^2$, $R_3 = k_3 n_F^4$, $R_4 = k_4 n_F^4$, $R_5 = k_5 n_O^2$, $R_6 = k_6 n_F^4$ are the reaction frequencies, and n_i is the concentration of i-th plasma component at the arbitrary point M on the surface as denoted in Fig. 1. Let us assume that $n_i(x,y) = n_{0,i}\Theta(x,y)/\pi$, where $n_{0,i}$ is the concentration of the i-th component in the plasma and $\Theta(x, y)$ is the limiting angle. The etching rate is equal to the sum of removal rates of Si^* atoms, SiO_2^* and SiF_4 molecules

$$V = h_0\left(\omega_1 c_1 + \omega_4 c_4 + \omega_5 c_5\right), \tag{12}$$

where $h_0 = 0.272$ nm is the monolayer thickness.

3. Results and discussion

The influence of chemical etching rate on the etched trench profile is most pronounced at initial stages of the etching process. Meanwhile, the physical sputtering rate does not depend on the etching time. The evolution of trench profile during RIE of silicon in $SF_6 + O_2$ plasma is shown in Fig. 2. It is observed that the lateral undercutting δ increases with the increase in etching time. The concentrations of $SF_6 + O_2$ plasma components, the reaction rate constants, and the desorption frequency, determined in previous work [10], are used for the calculation of etched trench profiles. The complete list of reaction rate constants and process frequencies used for the calculation of etched trench profiles is presented in Table I. The etched trench profiles at different O_2 content in the feed are shown in Fig. 3. It is observed that, at high O_2 content in the feed, the depth of etched trenches and lateral undercutting decrease.
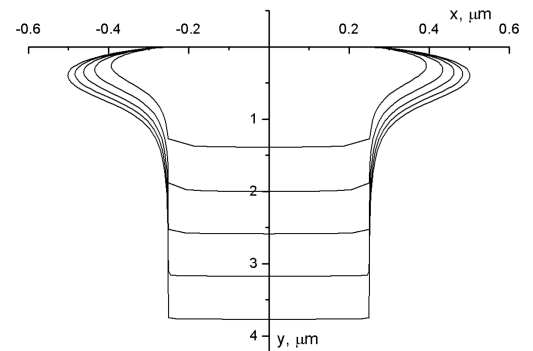

Fig. 2. The evolution of trench profile during RIE of silicon in $SF_6 + O_2$ plasma. The mask width 0.5 μm, the mask height 0.1 μm, the etching time 5 min, and O_2 content in the feed 10%. The trench profile is shown every minute.
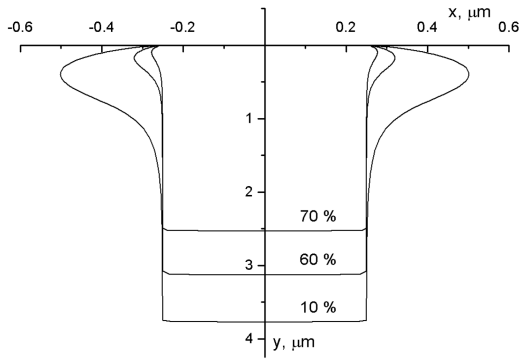
Fig. 3. The etched trench profiles at different values of O$_2$ content in the feed. The mask width 0.5 μm, the mask height 0.1 μm, and the etching time 5 min.

TABLE I

The reaction rate constants and process frequencies (in Hz) used for the calculation of etched trench profiles.

Rate constants		Frequencies	
G_2	2000	k_1	1.25×10^6
G_3	3000	k_2	100
ω_1	3500	k_3	1.00×10^4
ω_4	40	k_4	1.25×10^7
ω_5	8	k_5	1000
R_r	0	k_6	1.00×10^5

The difference in the surface composition on the side walls and trench bottom enables anisotropic etching. The side-wall passivation with SiO$_2$ molecules reduces the etching rate in the horizontal direction, while ion bombardment maintains the etching rate in the vertical direction. The aspect ratio $y_{max}/2x_{max}$ and etching anisotropy y_{max}/δ describe the shape of etched trenches. The dependences of the aspect ratio on O$_2$ content in the feed at different mask widths are shown in Fig. 4. With the increase in O$_2$ content, the aspect ratio initially decreases because the etching process becomes more isotropic due to the increased concentration of F atoms in SF$_6$ + O$_2$ plasma. With further increase in O$_2$ content, the side-wall passivation with SiO$_2$ molecules increases, and the aspect ratio starts to increase and reaches its maximum value. The appearance of maximum in the dependence is caused by the competition between F and O atoms for active Si surface sites in the trench bottom. Later, the aspect ratio starts to decrease due to the accumulation of SiO$_2$ molecules in the trench bottom.

The dependences of the etching anisotropy on O$_2$ content in the feed at different mask widths are shown in Fig. 5. At low O$_2$ content in the feed, the etching anisotropy reaches its minimum value due to the increased concentration of F atoms in SF$_6$ + O$_2$ plasma. The concentration of SiO$_2$ molecules is insufficient to passivate the side walls completely. Both the aspect ratio
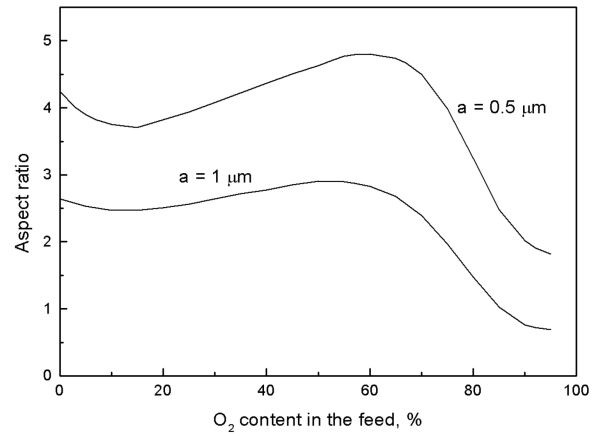

Fig. 4. The dependences of the aspect ratio on O$_2$ content in the feed at different mask widths. The mask height 0.1 μm and the etching time 5 min.
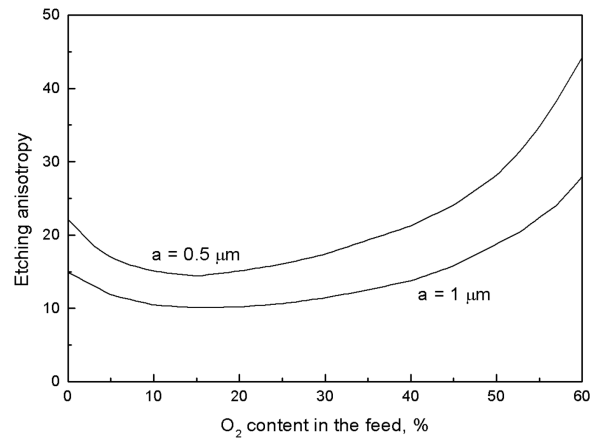

Fig. 5. The dependences of the etching anisotropy on O$_2$ content in the feed at different mask widths. The mask height 0.1 μm and the etching time 5 min.

and etching anisotropy increase with the decrease in the mask width. Theoretical results indicate that chemical interplay between F and O atoms on the side walls does not depend on the mask width. The dependence of maximum concentration of SiO$_2$ molecules on the side walls on O$_2$ content in the feed is shown in Fig. 6. It is important to note that concentration of SiO$_2$ molecules in the trench bottom is negligible in this range of O$_2$ content in the feed.

Inverse RIE lag takes place when the etched trench depth increases with the decrease in the microstructure width. At high O$_2$ content in the feed, the concentration of O atoms in SF$_6$ + O$_2$ plasma is much higher than the concentration of F atoms. Therefore, the etching rate in the vertical direction is easily suppressed by SiO$_2$ molecules. The evolution of trench profile at high O$_2$ content in the feed is shown in Fig. 7. Due to the uneven flux distribution of reactive atoms in the trench
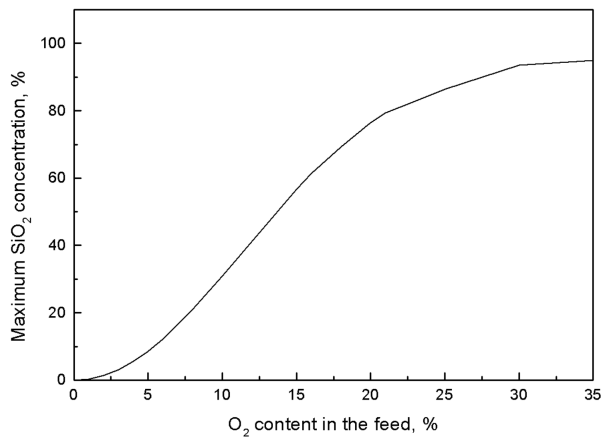
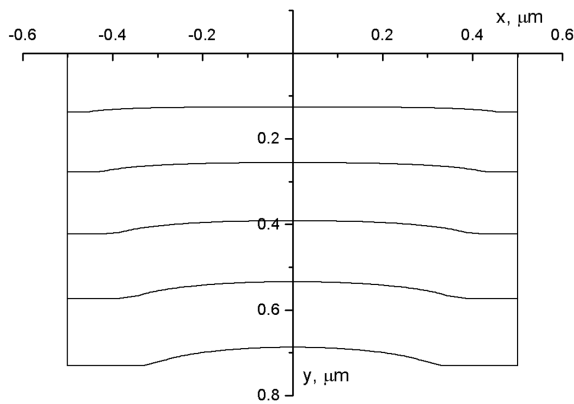Fig. 6. The dependence of maximum concentration of SiO_2 molecules on the side walls on O_2 content in the feed.

Fig. 7. The evolution of trench profile during RIE of silicon in $SF_6 + O_2$ plasma. The mask width 1 μm, the mask height 0.1 μm, the etching time 5 min, and O_2 content in the feed 80%. The trench profile is shown every minute.

bottom SiO_2 molecules tend to accumulate in the trench center rather than in trench edge. This results in the microtrenching because Si atoms have higher sputtering yield than SiO_2 molecules. The obtained results are supported by the experimental measurements [11] and theoretical calculations [12].

4. Conclusions

The shape of etched trenches is described using the aspect ratio and etching anisotropy. With the increase in O_2 content, the aspect ratio and etching anisotropy initially decrease due to the increased concentration of F atoms in $SF_6 + O_2$ plasma. The concentration of SiO_2 molecules is insufficient to passivate the side walls completely. With further increase in O_2 content, the sidewall passivation with SiO_2 molecules increases, and the aspect ratio and etching anisotropy start to increase. At high O_2 content, the aspect ratio starts to decrease due to the increased concentration of SiO_2 molecules in the trench bottom. The accumulation of SiO_2 molecules in the trench bottom results in the inverse RIE lag.

References

[1] H.F. Winters, D.B. Graves, D. Humbird, S. Tougaard, *J. Vac. Sci. Technol. A* **25**, 96 (2007).

[2] M.J. de Boer, J.G.E. Gardeniers, H.V. Jansen, E. Smulders, M.J. Gilde, G. Roelofs, J.N. Sasserath, M. Elwenspoek, *J. Microelectromech. Syst.* **11**, 385 (2002).

[3] R. Dussart, T. Tillocher, P. Lefaucheux, M. Boufnichel, *J. Phys. D Appl. Phys.* **47**, 123001 (2014).

[4] A. Burtsev, Y.X. Li, H.W. Zeijl, C.I.M. Beenakker, *Microelectron. Eng.* **40**, 85 (1998).

[5] K.A. Alshaltami, M. Morshed, C. Gaman, J. Conway, S. Daniels, *J. Vac. Sci. Technol. A* **35**, 031307 (2017).

[6] I. Sakai, N. Sakurai, T. Ohiwa, *J. Vac. Sci. Technol. A* **29**, 021009 (2011).

[7] P. Dixit, S. Vähänen, J. Salonen, P. Monnoyer, *ECS J. Solid State Sci. Technol.* **1**, P107 (2012).

[8] M. Ashraf, S.V. Sundararajan, G. Grenci, *J. Micro /Nanolith. MEMS MOEMS* **16**, 034501 (2017).

[9] E. Babaei, M. Gharooni, S. Mohajerzadeh, E.A. Soleimani, *J. Micromech. Microeng.* **28**, 075003 (2018).

[10] R. Knizikevičius, *Acta Phys. Pol. A* **117**, 478 (2010).

[11] T. Lill, M. Grimbergen, D. Mui, *J. Vac. Sci. Technol. B* **19**, 2123 (2001).

[12] K. Ono, H. Ohta, K. Eriguchi, *Thin Solid Films* **518**, 3461 (2010).